nature nanotechnology

ARTICLES

PUBLISHED ONLINE: 30 NOVEMBER 2015 | DOI: 10.1038/NNANO.2015.276

An ultrabright and monochromatic electron point source made of a LaB_6 nanowire

Han Zhang[1]*, Jie Tang[1,2]*, Jinshi Yuan[1], Yasushi Yamauchi[1], Taku T. Suzuki[1], Norio Shinya[1], Kiyomi Nakajima[1] and Lu-Chang Qin[3]

Electron sources in the form of one-dimensional nanotubes and nanowires are an essential tool for investigations in a variety of fields, such as X-ray computed tomography, flexible displays, chemical sensors and electron optics applications. However, field emission instability and the need to work under high-vacuum or high-temperature conditions have imposed stringent requirements that are currently limiting the range of application of electron sources. Here we report the fabrication of a LaB_6 nanowire with only a few La atoms bonded on the tip that emits collimated electrons from a single point with high monochromaticity. The nanostructured tip has a low work function of 2.07 eV (lower than that of Cs) while remaining chemically inert, two properties usually regarded as mutually exclusive. Installed in a scanning electron microscope (SEM) field emission gun, our tip shows a current density gain that is about 1,000 times greater than that achievable with W(310) tips, and no emission decay for tens of hours of operation. Using this new SEM, we acquired very low-noise, high-resolution images together with rapid chemical compositional mapping using a tip operated at room temperature and at 10-times higher residual gas pressure than that required for W tips.

The functionality of nanoscale field emitters has been utilized in a broad range of applications[1–8]. The fundamental property of a field emitter that determines the highest achievable brightness with the lowest energy spread is the low work function (ϕ) of the emitter material[9]. The best electron source used for high-resolution scanning transmission electron microscopes (STEM) is made from (310) oriented tungsten with a high ϕ of 4.5 eV. Even operated in an ultrahigh vacuum (UHV), the inevitable instabilities, including a temporal decay of emission current (long term instability) and a stochastic current fluctuation (short term instability), present a technological challenge to general application[10,11]. As a result, it has forced the industry to choose the more stable Schottky electron emitter, which unfortunately compromises both the brightness and coherence of the electron beam[12,13]. The high ϕ value of tungsten also limits further advancement of resolution for an STEM equipped with the most advanced spherical aberration correctors[14,15].

Lanthanum hexaboride (LaB_6) has a ϕ of 2.07 eV and has been utilized as thermionic electron source for decades[16,17]. Although intense efforts have been made for decades owing to the envisaged huge potential applications in electron beam imaging, no stable LaB_6 field emitter could be realized. A rapid emission decay (>90% decay in a few minutes) was commonly observed and it has led to a conviction that a LaB_6 field emission source is impractical[18,19].

Here we report a stable LaB_6 field emitter that can be operated at a high current density for tens of hours without decay. It is enabled by a nanostructure with only a few La atoms situated on the tip of a chemically grown single-crystalline LaB_6 nanowire (NW). An ultrahigh brightness and beam monochromaticity have been verified experimentally and compared with the best contemporary electron sources. Using this new electron source, we also present a new cold field emission SEM with significant improvements in both imaging and analytical capabilities.

Fabrication of the LaB_6 electron point source

The LaB_6 NWs used in this study are <100> oriented single crystals as shown in Fig. 1a. An NW with thickness of 50–80 nm and length of 10–20 μm was picked up from the substrate and transferred onto the tip of a W needle using a home-built nanomanipulator (inset of Fig. 1a). A modified SEM was used to produce a carbon pad, fixing the nanowire on the W tip (Fig. 1b). The finished emitter structure is shown in Fig. 1c and its inset. Excessive LaB_6 was removed on the tip surface using a field evaporation process[20]. Figure 1d shows the smooth hemispherical tip produced from the original NW shown in the left inset. This process results in no damage to the rest of the NW, as indicated by the perfect diffraction pattern shown in the right inset. A significant difference between this LaB_6 NW and those reported previously is that the surface of the LaB_6 NW is clean[20–24]. No amorphous substance was observed (Fig. 1e) and no elements other than La and B were observed in the energy dispersive X-ray (EDX) spectra. To set the ϕ of the LaB_6 surface, a positive electric field was applied to activate the positively charged La atoms on the apical surface, as illustrated in Fig. 1f. This process was monitored *in situ* using field-ion microscopy (FIM). The upper inset is an FIM image of the NW tip showing the absence of La atoms before field actuation[20]. The emergence of a La atom layer after field activation is shown in the FIM image as the lower inset (See Supplementary Figs 1 and 2). On applying a low voltage of a few hundred volts, a highly collimated electron beam was generated from the atomic La layer with a beam divergence of 5° (Fig. 2g). The upper inset is a field emission microscope (FEM) image of the emission beam intercepted by a phosphor screen. The beam divergence is much narrower than the 70° angle from a contemporary W(310) emitter[25].

Electron optical characterization of LaB_6 point source

Before measurement, the central emission spot was aligned with a 0.002 sr probe aperture on the imaging plate in the field emission

[1]National Institute for Materials Science, Tsukuba, Ibaraki 305-0047, Japan. [2]Graduate School of Pure and Applied Science, University of Tsukuba, Tsukuba, Ibaraki 305-8577, Japan. [3]Department of Physics and Astronomy, University of North Carolina at Chapel Hill, Chapel Hill, North Carolina 27599-3255, USA. *e-mail: zhang.han@nims.go.jp; tang.jie@nims.go.jp

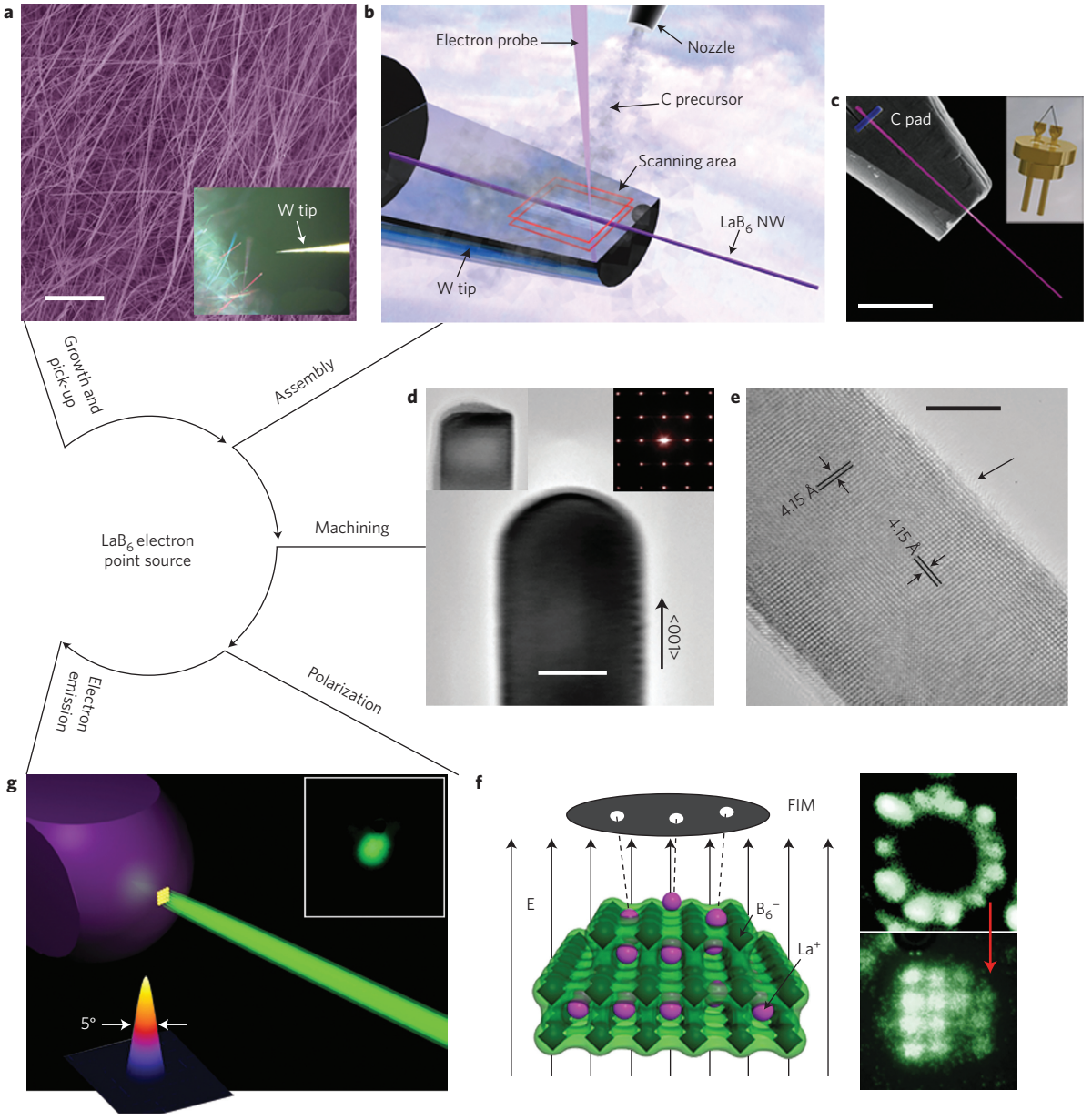

Figure 1 | Nanofabrication of a LaB_6 electron point source. a, SEM image showing LaB_6 NWs uniformly grown on a single crystal LaB_6 (100) substrate. Scale bar, 10 μm. Inset: optical image as a LaB_6 nanowire is picked up by a W tip. **b**, Illustration showing the electron beam deposition process to fix a LaB_6 NW onto a W needle. **c**, SEM image showing the finished LaB_6 NW emitter and the complete emitter assembly used for field-emission SEM. **d**, Hemispherical NW tip produced by field evaporation. Scale bar, 30 nm. Left inset:assembled tip. Right inset: the electron diffraction pattern of the tip after field evaporation, showing that perfect crystallinity is maintained. **e**, High-resolution TEM image showing the clean surface of the LaB_6 NW synthesized by this method. Scale bar, 5 nm. **f**, The activation process, where electric field is used to set the positively charged La atoms onto the tip surface of a LaB_6 NW. Top inset: field-ion microscope image of the NW before field activation. Bottom inset: NW after field activation with La atoms on top. **g**, Schematic illustrating the localized electron emission from the La layer as revealed in **f**. Left inset: the spatial distribution profile of the emitted electron beam. Right inset: the field emission pattern recorded on a phosphor screen.

microscope (FEM), so that a portion of the current emitted from the LaB_6 NW is collected as the probe current I_p and the current emitted from the whole nanowire is recorded as the total current I_t (see Supplementary Fig. 5). The set-up follows a simple needle-to-plate geometry.

The dependence of field emission current I on extraction voltage U for a metallic emitter can be described by the Fowler–Nordheim (F–N) formula[26]:

$$I = S \cdot J = aS\beta^2 \frac{U^2}{\phi} \exp\left[-b\frac{\phi^{3/2}}{\beta U}\right](A/m^2) \quad (1)$$

where S is the physical emission area, J is the areal current density, β is the field enhancement factor, and $a = 1.54 \times 10^{-6}$ and $b = 6.83 \times 10^9$ are constants. The measured I_p–U is plotted in Fig. 2a with the y axis being I', the current density per solid angle normalized with the electron potential. The maximum recorded I' before ion bombardment-induced instability is 19 μA sr^{-1} kV^{-1} for the LaB_6 NW at the test chamber vacuum. This current density is generated from an equivalent physical source size S_p of only 0.12 nm^2, which is determined using the probe-hole FIM technique (see Supplementary Fig. 5). The maximum I' for the LaB_6 NW is nearly 4 times of that for a

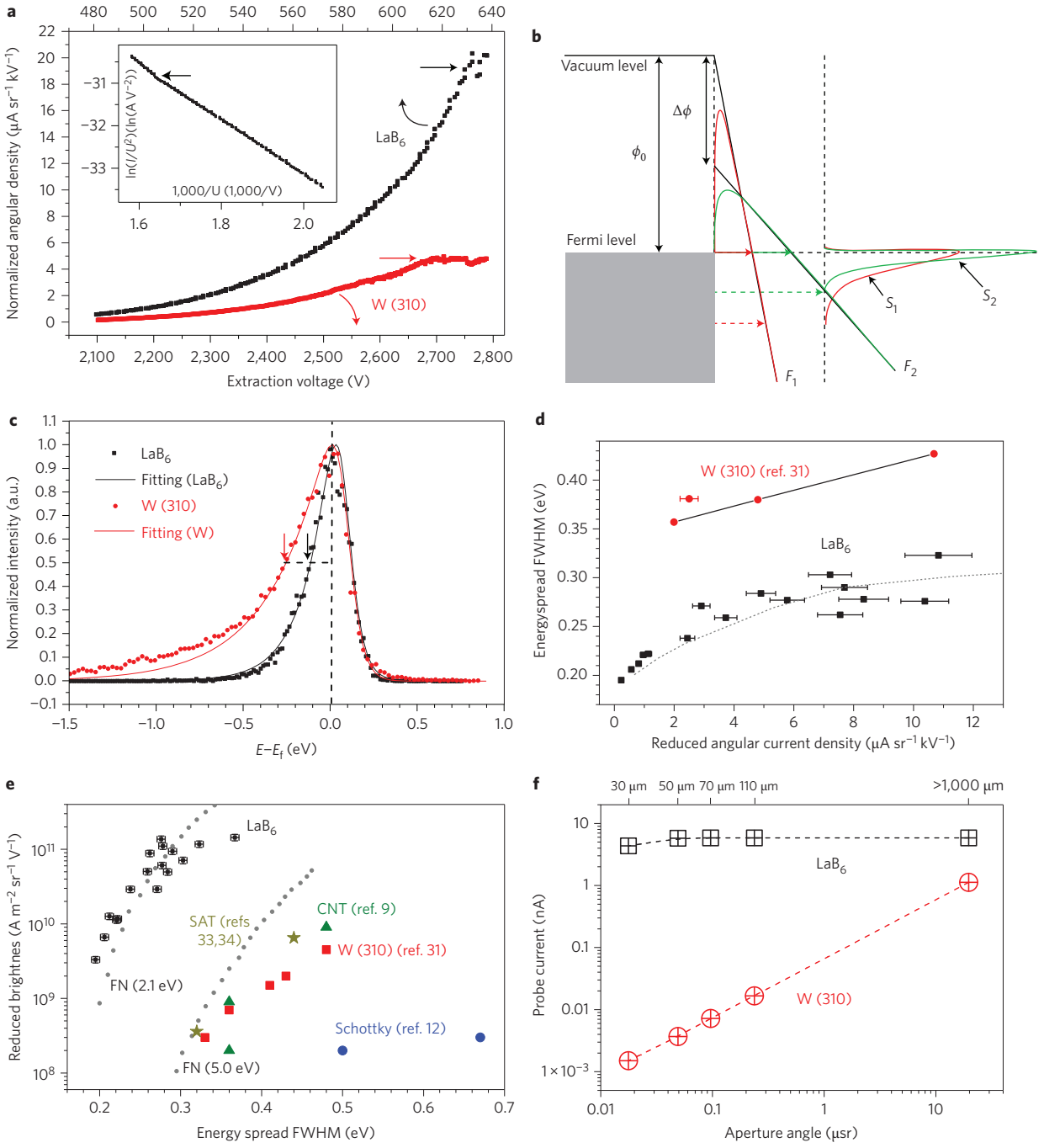

Figure 2 | Electron optical characterization of the LaB_6 NW field emitter. a, The dependence of normalized angular current density on extraction voltage with maximum value limited by emission instability. Inset: F-N plot showing linearity with a transition point at high current density. **b**, Energy band showing the origin of the low work function for a LaB_6 NW and its influence on emission current density and beam monochromaticity. **c**, Electron energy distribution from a LaB_6 NW and a W(310) tip emitting at current densities of 1.8×10^{10} A m^{-2} and 3.6×10^{9} A m^{-2}, respectively. **d**, Dependence of energy spread ΔE on reduced angular current density I' and its comparison with a W(310) emitter. **e**, Reduced brightness versus energy spread for LaB_6 NWs and other high-brightness electron sources. The uncertainty in the x axis is ±0.005 eV due to the resolution of energy analyser. Uncertainty in the y axis is ±10% in determination of physical source size. The distribution of data agrees well with that predicted by the F-N theory. **f**, Probe current recorded passing through a series of apertures located 20 cm below the electron gun exit in a field emission SEM. Aperture diameter is labelled on the top x axis.

W(310) needle emitter that has a much larger emission area (2–5 nm^2). The robustness against ion bombardment of the LaB_6 NW indicates the high strength of the La–B bonds on surface. Equation (1) can also be re-written as

$$\ln\left(\frac{I}{U^2}\right) = \frac{m}{U} + n,\ m = -\frac{b\phi^{3/2}}{\beta},\ n = \ln\left(\frac{aS\beta^2}{\phi}\right) \qquad (2)$$

Plotting $\ln(I/U^2)$ against $1/U$ thus generates a straight line with slope m and the y-intercept n as defined above. Such a modified F–N plot is shown in the inset of Fig. 2a. A perfect linearity is conserved from low current density up to a transition point at 14 μA sr^{-1} kV^{-1}, which indicates an onset of emission contribution from the B-covered nanowire base[27].

Assuming a work function ϕ_0 for a B-terminated LaB_6 NW tip without the surface La atomic layer, the corresponding electron

beam energy distribution has the form of S_1 as shown in Fig. 2b (at field F_1). The addition of the positively charged La atoms on the surface lowers the near surface vacuum potential, thus effectively reduces ϕ_0 by $\Delta\phi$. When a lower field F_2 is applied, the new tunneling probability (roughly depends on the area under barrier curve)[26] at the Fermi level is slightly higher than that created by F_1, therefore results in a higher emission current density. More importantly, because F_2 creates a quicker decay of tunneling probability with respect to energy below Fermi level, the new energy distribution S_2 has a higher monochromaticity than S_1.

This mechanism can be verified through measurement of the energy distribution of the emitted electrons. Figure 2c shows the normalized beam intensity with respect to electron energy relative to the Fermi level for the LaB_6 NW. The low energy tail for LaB_6 NWs is 49% shorter at half maximum than that for a W(310) emitter measured at an areal current density, J, 1/5 that of the LaB_6 NW emitter (see Supplementary Fig. 6). Full width at half maximum (FWHM) is 0.24 and 0.38 eV for the LaB_6 NW and W(310) emitter, respectively. The LaB_6 NW spectrum corresponds to situation S_2 for a low ϕ emitter as compared to W(310) corresponding to S_1 with a high ϕ. As shown in Fig. 2b, for any given ϕ, the energy spread increases as the electric field is raised and emission current increases. This trend can be seen from Fig. 2d, where the energy spread for LaB_6 NWs increases from the lowest measured value of 0.195 eV as I' increases. They are all about 30% lower than W(310) emitters operated under the same values, due to a lower ϕ (see Supplementary Fig. 7).

Based on the I–U curve and energy distribution profile, the exact work function for LaB_6 NW is obtained with an average $\phi = 2.09 \pm 0.17$ eV for 6 emitters (Supplementary Information, Data Analysis section vii)[28]. This value is smaller than the value of 2.3 eV reported on the LaB_6 (100) thermionic emitter and is very close to the theoretical value of 2.07 eV obtained by *ab initio* calculations assuming an ideal material[17,29]. The extremely low ϕ of 2.1 eV means that, with an emission current density $\sim 1 \times 10^9$ A m^{-2}, the LaB_6 NW emitter would only require less than 1/3 of the operation voltage for a carbon nanotube emitter with a ϕ of 5.1 eV (ref. 9).

Electron optical applications demand an electron source with the highest possible reduced brightness B_r (brightness normalized with beam energy) and lowest possible energy spread ΔE (ref. 14). Practical brightness is measured in our experiment by following $B_r = 1.44J/(\pi d)^2$[30], where d is transverse energy obtained by fitting the energy spectrum and J is areal current density obtained through $J = I_p/S_p$ (see Supplementary Table 1, Figs 5 and 9). The B_r values for LaB_6 NW emitters measured at different emission current densities are plotted in Fig. 2e against their ΔE values obtained as FWHM from the energy distribution spectra. The W(310) values are taken from the literature deduced by following the practical brightness definition[31]. The grey square points are numerically calculated B_r–ΔE values based on $\phi = 2.1$ and 5.0 eV, respectively. Our data points roughly follow a logarithmic curve and distributed along the F–N predicted values. It can be seen that all B_r values from cold field emitters on this chart roughly start deviating below the F–N prediction from a ΔE value around 0.34 eV. This is attributed to the increase of transverse energy d as a result of the coulombic electron–electron interactions (Boersch effect)[32]. The fact that the lowest B_r that initiates the Boersch effect is much higher for LaB_6 NW than for W(310) should be a result of quicker electron spreading due to the much smaller emitter size (see Supplementary Fig. 8). The data in the chart distributes in three zones: Schottky emitter belongs to the lowest B_r zone, due to the low emission current density of thermionic emission[12]; W(310), carbon nanotube (CNT), and single atom tip (SAT) all roughly fall in the middle B_r zone because they are all cold field emitters and have similar work functions ($\sim 5 \pm 0.5$ eV)[9,31,33,34], and the LaB_6 NW emitter occupies the highest B_r zone with B_r values that differ by about 2 orders of magnitude compared with the middle B_r zone emitters for the same ΔE.

Stability of the field-emission LaB_6 electron point source

Figure 3a is a typical short-term stability profile of the LaB_6 NW electron probe current. The high-frequency current fluctuation of a field emitter is known as flicker noise, which originates from the constant adsorption/desorption of the residual gas molecules (see Supplementary Fig. 10a). The RMS noise ratio $\langle \Delta I^2 \rangle^{1/2}/I$ should be inversely proportional to a power of 1.5 of the emission surface area[35]. It suggests a noise ratio more than 1,000 times higher for the smaller LaB_6 NW than the larger W needle, if both have the same coverage of adsorbates. On the contrary, $\langle \Delta I^2 \rangle^{1/2}/I$ for the LaB_6 NW is only 0.32% compared with 7.2% for W(310) tested under the same vacuum condition. The contradiction between observation and theoretical prediction is explained by a completely inert surface of the LaB_6 NW, which is free of surface adsorption (see Supplementary Figures 3, 4, 10b and 11). When H_2 gas with a dose of 60 ml (10^{-9} torr × 60 s) was intentionally leaked into the chamber every other minute while the probe current I_p of the LaB_6 NW emitter was recorded continuously, as shown in Fig. 3c, the emission stability was clearly unaffected by the H_2 exposure up to a total dose of 660 ml. To further verify the inertness of the LaB_6 NW surface, one field emission I–V curve was recorded each day for a week without any surface cleaning operation. n, m, and I_p (at fixed U) values are extrapolated and plotted in Fig. 3b. Those quantities for LaB_6 deviate from the mean within 5% throughout the week-long test, whereas those for W(310) deviate between 20–80%, even after excluding the first day of data that deviates more than one order of magnitude from the rest. This proved an interesting combination of two mutually exclusive properties had been achieved: low ϕ and high chemical inertness[36,37].

SEM using an LaB_6 NW electron source

One LaB_6 NW emitter was installed in the electron gun of a cold field emission type SEM (trial tests were carried out on Hitachi SU8000 and home-modified JEOL JSM-6700F). In a comparison study using JSM-6700F, total emission currents of 45 nA and 20 μA were extracted from the LaB_6 NW emitter and the original W(310) emitter with extraction voltages of 500 V and 5,400 V, respectively. Electron beams from both emitters were accelerated to 15 kV and the probe current was collected directly behind a series of beam-limiting apertures set 20 cm below the electron gun exit without convergence by condenser lens. As shown in Fig. 2f, the probe current of the W emitter decreases proportionally against decreasing aperture area, indicating a fixed value of angular current density from a widespread beam. That of the LaB_6 NW emitter remained almost constant until the smallest aperture of 30 μm, indicating a collimated beam shape with ~30 μm waist diameter. The electron gun equipped with LaB_6 NW thus shows an ultrahigh angular current density of $\sim 2.4 \times 10^5$ μA sr^{-1}, which is ~1,000 and ~100 times greater than the electron guns with a W(310) emitter and a Schottky emitter, respectively[12].

To test the emission stability of the LaB_6 NW emitter in a working environment with a higher gas pressure, air was released into the vacuum chamber till the gas pressure of the intermediate gun chamber reached 3×10^{-6} Pa, with a similar pressure to a Schottky electron gun. Figure 3d shows recorded current measurements for the LaB_6 NW emitter for a test duration of 5 h. Both the total and probe currents showed the same non-decay profile and have synchronized small step-type variations. This verified the fact that majority of the electron emission is confined to the (100) tip facet of the LaB_6 NW. As a comparison, although intermediate gun chamber pressure was kept around 1×10^{-7} Pa during test, the W(310) emitter still followed a rapid current decay after flashing cleaning. Extraction voltage was raised from

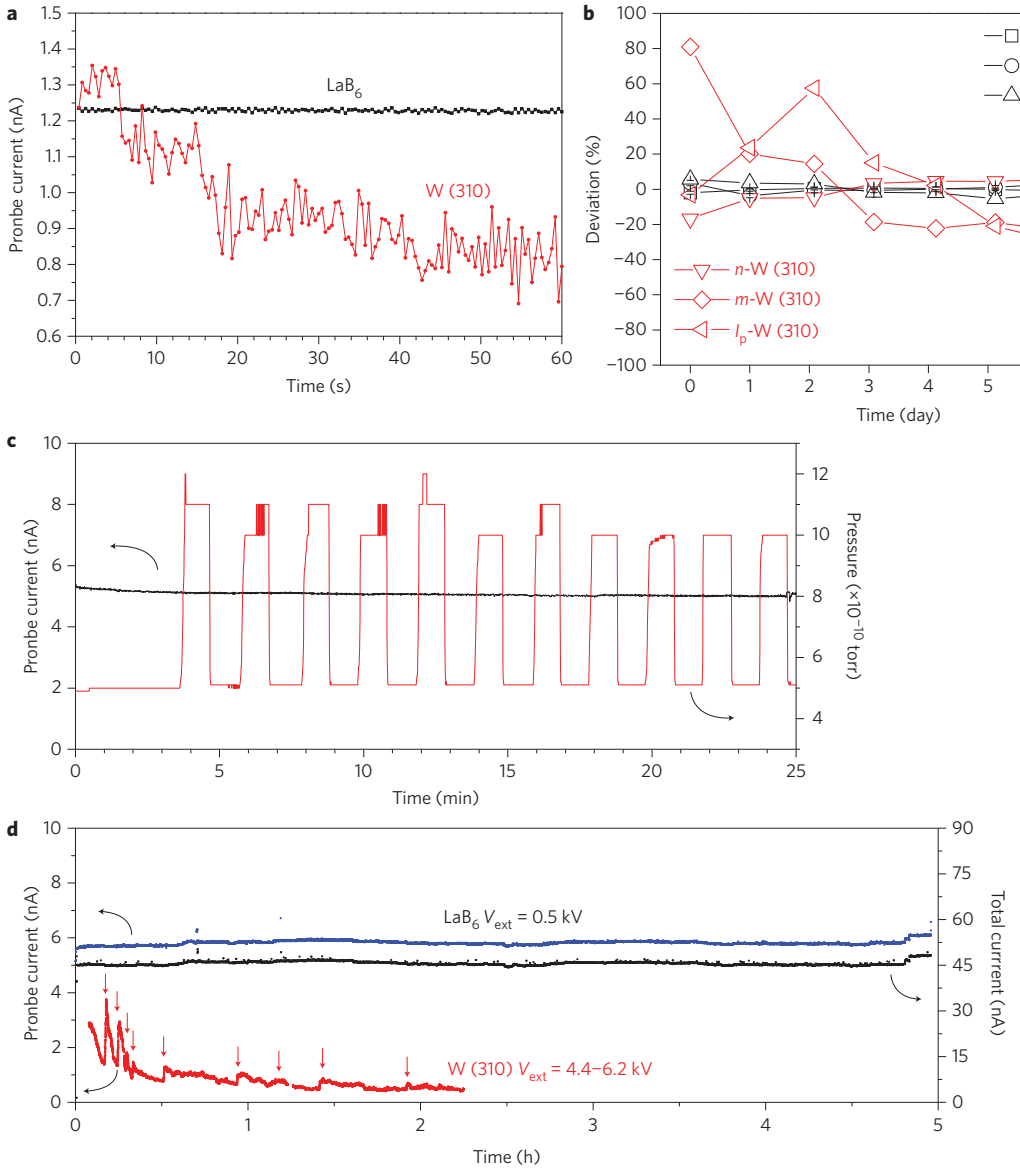

Figure 3 | Stability of field-induced electron emission. a, Emission noise profile with implication of surface coverage with adsorbates. **b**, *n*, *m*, and I_p deviation from mean values measured for 7 days, indicating little change in ϕ and field enhancement for a LaB_6 NW. **c**, Emission probe current profile of a LaB_6 NW emitter during intentional exposure to H_2 gas. **d**, Long-term stability profiles measured in a field emission SEM with intermediate gun chamber pressures of 3×10^{-7} Pa for the LaB_6 NW emitter and 1×10^{-7} Pa for W(310) emitter. Arrows indicate extraction voltage raises to keep a total emission current of 20 μA for the W emitter.

4.3 kV to 6.2 kV nine times during the 2 h of test duration. Though the total emission was maintained at 20 μA, probe current decayed constantly and remained below 1 nA for most of the test period. One SEM image of a gold particle-on-carbon specimen was taken by using the LaB_6 NW emitter with a high probe current of 5.6 nA. (Fig. 4c) The area containing a resolved gold particle of 7.8 nm in width is displayed in the inset. The small electron probe size of a few nanometres, even under high probe current, is verified. The stable current profile and high probe current of the LaB_6 NW emitter therefore demonstrate its suitability in micro-beam analytical applications that were previously considered incompatible with a cold field emission gun. Figure 4d is an energy dispersive X-ray compositional mapping of a multilayer film specimen acquired using the LaB_6 NW emitter. The probe current was lowered to 1.9 nA to ensure the best efficiency for the Si(Li) detector. A total count of 2×10^6 was collected in 10 min until all of the compositional details became adequately discernible. It takes more than double the acquisition time for the original W field emitter, even with the help of a beam condenser lens tuned to maximum power.

Figure 4a is an image of the acceleration electrode in the objective lens taken when the electron beam was scanned with only the upper scanner from the scanner pair. The upper half of the image, taken using the LaB_6 NW emitter, only shows grainy shot noise from the secondary electron detector. The lower half of the image, taken using the W emitter, displays alternating stripes of bright and dark contrast besides the detector shot noise. This type of noise is a result of flicker noise from the W emission current and its amplitude becomes greater with elapse of emission time after tip flashing. By modulating the detector signal with recorded emission current, however, the stripes could be artificially reduced, although interruption of emission after several hours of operation is still inevitable when subsequent flashing becomes necessary. The LaB_6 NW emitter is free from such emission fluctuation and

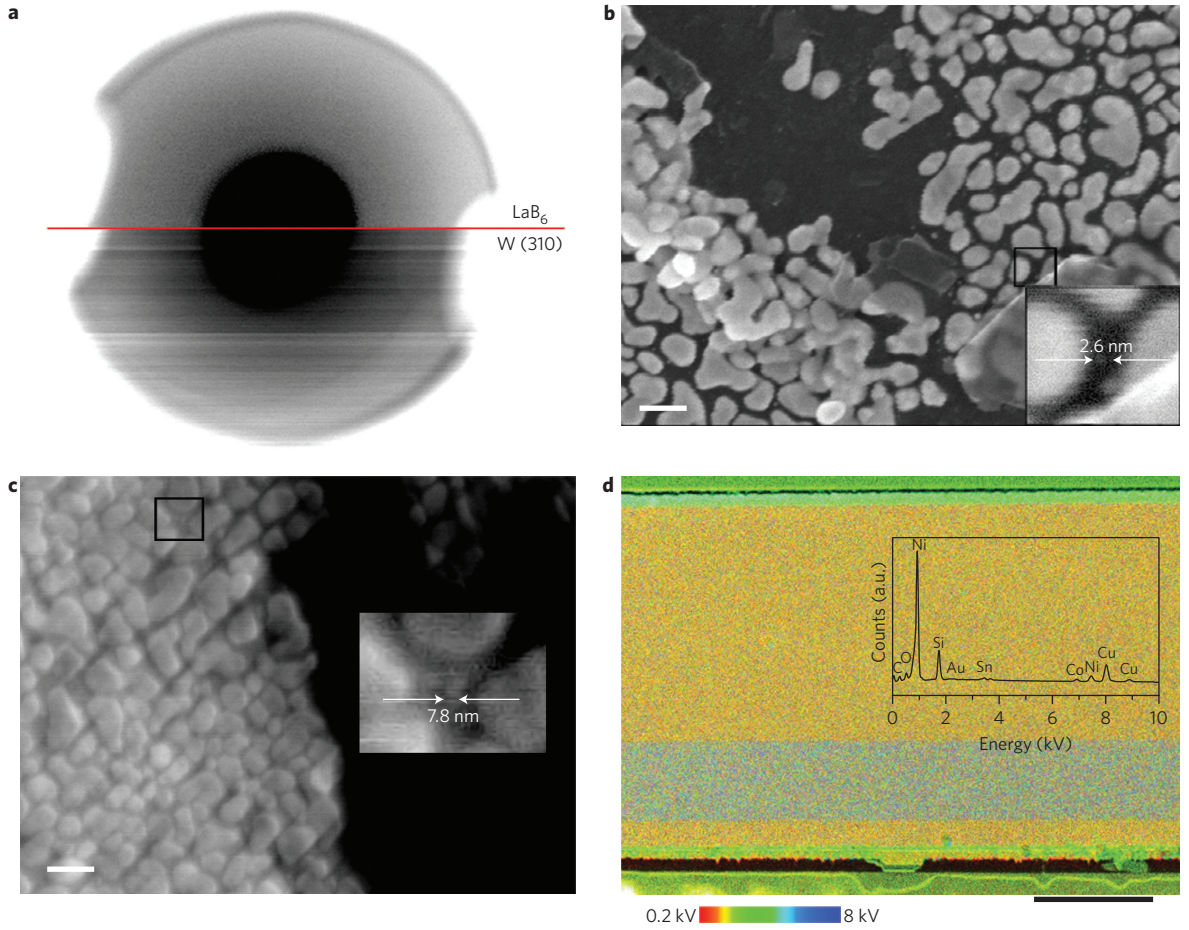

Figure 4 | A field emission SEM with a LaB_6 nanowire electron point source. a, Signal noise comparison for imaging the acceleration electrode in the SEM objective lens using the LaB_6 NW emitter and W emitter, respectively. Raw images without noise canceller modulation. **b**, A low-voltage image taken from a gold particle-on-carbon specimen using the LaB_6 NW emitter. Scale bar, 100 nm, magnification ×100,000, voltage 5.0 kV, working distance 3.3 mm. Inset: enlarged view of a particle imaged at ×200,000 magnification. **c**, Image taken from the same sample using a high probe current of 5.6 nA without the use of a condenser lens. Scale bar, 100 nm, magnification ×100,000, voltage 15.0 kV, working distance 3.0 mm. Inset: enlarged view of region indicated by the black rectangle. **d**, A composite image made by combining the secondary electron signal with the X-ray signal. Scale bar, 30 μm. The colour gradient indicates the energy of the X-ray acquired. Inset: the X-ray spectrum accumulated from the entire mapped area.

therefore could offer continuous operation with noise-free raw images. Figure 4b is a low-voltage high-resolution image of a gold particle-on-carbon specimen where a small Au particle of 2.6 nm in size was clearly resolved. Using the B_r and ΔE values for the LaB_6 NW emitter, the electron probe size at the current imaging condition is calculated to be 2.2 nm, which agrees very well with the experimental result (see Supplementary Table 1).

Conclusions

We have developed a new field emission electron point source using a single LaB_6 nanowire. The source has an extremely low work function and emits at a high current density with very low flicker noise and no current decay, as a result of an inert surface free from chemisorption of residual gas. A cold field emission SEM was installed with this emitter and demonstrated significant advantages over W(310) emitter in both imaging and analytical capabilities. It is desirable to engineer electron gun structures that can accommodate our electron point source. For electron optics applications, for example, these guns should be able to accurately align with the optical axis and accelerate the electron beam directly after emission to remove possible coulomb interactions, which currently prevent ultimate brightness from being reached. In parallel, efforts should be devoted to expand the advantages from individual LaB_6 nanowires to LaB_6 nanowire films and regularly patterned LaB_6 nanowire arrays.

Moreover, combining the low operation voltage and chemical inertness of our LaB_6 nanowire emitter with available technologies in large-scale field emission devices (lamps and displays) is expected to improve the resolution of microcomputed tomography and electron microscopes.

Methods

Methods and any associated references are available in the online version of the paper.

Received 27 November 2012; accepted 20 October 2015; published online 30 November 2015

References

1. Ghosh, P. *et al.* Transparent and flexible field electron emitters based on the conical nanocarbon structures. *J. Am. Chem. Soc.* **132,** 4034–4035 (2010).
2. Choi, W. *et al.* Fully sealed high brightness carbon nanotube field emission display. *Appl. Phys. Lett.* **75,** 3129–3131 (1999).
3. Sugie, H. *et al.* Carbon nanotubes as electron source in an x-ray tube. *Appl. Phys. Lett.* **78,** 2578–2580 (2001).
4. Lee, Y. *et al.* Carbon nanotube based x-ray sources: applications in pre-clinical and medical imaging. *Nucl. Instrum. Meth. A* **648,** S281–S283 (2011).
5. Modi, A., Koratkar, N., Lass, E., Wei, B. & Ajayan, P. Miniaturized gas ionization sensors using carbon nanotubes. *Nature* **424,** 171–174 (2003).
6. Sadeghian, R. & Islam, M. Ultralow voltage field ionization discharge on whiskered silicon nanowires for gas-sensing applications. *Nature Mater.* **10,** 135–140 (2011).

7. de Jonge, N., Lamy, Y., Schoots, K. & Oosterkamp, T. High brightness electron beam from a multi-walled carbon nanotube. *Nature* **420,** 393–395 (2002).
8. Houdellier, F., Masseboeuf, A., Monthioux, M. & Hytch, M. New carbon cone nanotip for use in a highly coherent cold field emission electron microscope. *Carbon* **50,** 2037–2044 (2012).
9. de Jonge, N., Allioux, M., Oostveen, J., Teo, K. & Milne, W. Optical performance of carbon nanotube electron sources. *Phys. Rev. Lett.* **94,** 186807 (2005).
10. Yeong, K. & Thong, J. Life cycle of a tungsten cold field emitter. *J. Appl. Phys.* **99,** 104903 (2006).
11. Kasuya, K., Katagiri, S. & Ohshima, T. Stabilization of a tungsten <310> cold field emitter. *J. Vac. Sci. Technol. B* **28,** L55–L60 (2010).
12. Schwind, G., Magera, G. & Swanson, L. Comparison of parameters for schottky and cold field emission sources. *J. Vac. Sci. Technol. B* **24,** 2897–2901 (2006).
13. Intaraprasonk, V., Xin, H. & Muller, D. Analytic derivation of optimal imaging conditions for incoherent imaging in aberration corrected electron microscopes. *Ultramicroscopy* **108,** 1454–1466 (2008).
14. Pennycook, S. & Nellist, P. *Scanning Transmission Electron Microscopy* (Springer, 2011).
15. Krivanek, O. *et al.* Atom by atom structural and chemical analysis by annular dark field electron microscopy. *Nature* **464,** 571–574 (2010).
16. Ahmed, H. & Broers, A. Lanthanum hexaboride electron emitter. *J. Appl. Phys.* **43,** 2185–2192 (1972).
17. Uijttewaal, M., Wijs, G. & Groot, R. Ab initio and work function and surface energy anisotropy of LaB_6. *J. Phys. Chem. B* **110,** 18459–18465 (2006).
18. Futamoto, M., Hosoki, S., Okano, H. & Kawabe, U. Field emission and field ion microscopy of lanthanum hexaboride. *J. Appl. Phys.* **48,** 3541–3546 (1977).
19. Nagata, H., Harada, K. & Shimizu, R. Thermal field emission observation of single crystal LaB_6. *J. Appl. Phys.* **68,** 3614–3618 (1990).
20. Zhang, H. *et al.* Nanostructured LaB_6 field emitter with lowest apical work function. *Nano Lett.* **10,** 3539–3544 (2010).
21. Zhang, H., Zhang, Q., Tang, J. & Qin, L. Single crystalline LaB_6 nanowires. *J. Am. Chem. Soc.* **127,** 2862–2863 (2005).
22. Zhang, H. *et al.* Field emission of electrons from single LaB_6 nanowires. *Adv. Mater.* **18,** 87–91 (2006).
23. Brewer, J., Deo, N., Wang, Y. & Cheung, C. Lanthanum hexaboride nanoobelisks. *Chem. Mater.* **19,** 6379–6381 (2007).
24. Amin, S., Li, S., Roth, J. & Xu, T. Single crystalline alkaline earth metal hexaboride one dimensional (1D) nanostructures: synthesis and characterization. *Chem. Mater.* **21,** 763–770 (2009).
25. Fujita, S. Electron gun technologies for high resolution electron microscopes. *J. Vac. Soc. Jpn* **55,** 64–72 (2012).
26. Fursey, G. *Field Emission In Vacuum Microelectronics* (Kluwer Academic, 2005).
27. Qian, W., Scheinfein, M. & Spence, J. Brightness measurement of nanometer sized field emission electron sources. *J. Appl. Phys.* **73,** 7041–7045 (1993).
28. de Jonge, N. *et al.* Characterization of the field emission properties of individual thin carbon nanotubes. *Appl. Phys. Lett.* **85,** 1607–1609 (2004).
29. Nishitani, R. *et al.* Surface structures and work functions of the LaB_6 (100), (110) and (111) clean surfaces. *Sur. Sci.* **93,** 535–549 (1980).
30. Bronsgeest, M., Barth, J., Swanson, L. & Kruit, P. Probe current, probe size, and the practical brightness for probe forming systems. *J. Vac. Sci. Technol. B* **26,** 949–955 (2008).
31. Swanson, L. & Schwind, G. A review of the cold field electron cathode. *Adv. Imag. Elect. Phys.* **159,** 63–98 (2009).
32. Orloff, J. *Handbook of charged particle optics* (CRC Press, 2009).
33. Chang, C., Kuo, H., Hwang, I. & Tsong, T. A fully coherent electron beam from a noble metal covered W(111) single atom emitter. *Nanotechnology* **20,** 115401 (2009).
34. Oshima, C., Rokuta, E., Itagaki, T., Ishikawa, T. & Cho, B. Demountable single atom electron source. *e-J. Surf. Sci. Nanotech.* **3,** 412–416 (2005).
35. Swanson, L. & Martin, N. Field electron cathode stability studies: zirconium/tungsten thermal field cathode. *J. Appl. Phys.* **46,** 2029–2050 (1975).
36. Toda, Y. *et al.* Work function of a room temperature stable electride $[Ca_{24}Al_{28}O_{64}]^{4+}(e^-)_4$. *Adv. Mater.* **19,** 3564–3569 (2007).
37. Zhou, Y. *et al.* A universal method to produce low work function electrodes for organic electronics. *Science* **336,** 327–332 (2012).

Acknowledgements

This work was partially supported by the Development of System and Technology for Advanced Measurement and Analysis, Japan Science and Technology Corporation (JST) and the Nanotechnology Network Project of the Ministry of Education, Culture, Sports, Science, and Technology (MEXT), Japan. The authors also wish to thank Hitachi High-Technologies Corporation for assistance in this project.

Author contributions

H.Z., J.T. and L.C.Q. conceived the idea of the study and performed data analysis. H.Z. carried out the main experiments. H.Z., J.T. and L.C.Q. wrote the manuscript. J.T. supervised the project. J.Y. participated in component fabrication. Y.Y. participated in component design and result analysis. T.T.S. participated in the electron energy analyser construction. K.N. carried out electron/ion beam fabrication. N.S. participated in data analysis.

Additional information

Supplementary information is available in the online version of the paper. Reprints and permissions information is available online at www.nature.com/reprints. Correspondence and requests for materials should be addressed to H.Z. and J.T.

Competing financial interests

The authors declare no competing financial interests.

Methods

Nanowire synthesis. The synthesis was carried out using a chemical-vapor-deposition approach. $LaCl_3$ powder (99.99%, Aldrich) was placed in a graphite crucible up-stream of a quartz tube heated in a furnace. A graphite tube was utilized to reach the centre of the quartz tube where a Pt-coated LaB_6 single crystal (100) substrate was placed to host nanowire growth. The inner area of the quartz tube was also protected by a graphite sheath. The reaction zone was first evacuated to the lowest pressure possible with a rotary pump. A hydrogen pressure of 0.1 atm was then produced and kept throughout the synthesis. When the reaction zone was heated to a temperature of 1400 K, BCl_3 gas (99.9%, Aldrich) was introduced through the graphite tube with a flow rate of 5 sccm for 5 min (refs 21,22).

Single NW emitter assembly. The LaB_6 substrate with grown LaB_6 NWs was placed under an optical microscope (Keyence VHX). A W needle etched from a 0.1 mm W wire was controlled by a 3D micrometer to approach individual LaB_6 NWs. The needle tip was previously cut with a focused ion beam to form a flat area 5 μm × 10 μm so its surface adheres well to the LaB_6 NWs, which are under 100 nm in diameter, through van der Waals force. After a single LaB_6 NW was broken off from the growth substrate and adhered onto the needle, electron-beam-induced carbon deposition was used to fix the nanowire to a carbon pad[20].

Ion emission and electron emission. The single NW emitter was installed in a vacuum chamber with a base pressure of 10^{-10} torr. A micro-channel plate/phosphor screen assembly is placed directly in front of the emitter at a distance of 50 mm. It serves both as an anode and is used to form intensified ion and electron images. During ion/electron emission, a high voltage of either polarity is applied to the emitter and the imaging assembly is grounded. Probe current is collected with a Faraday cup, which is placed behind the channel plate probe hole of 2 mm in diameter. An electrometer (Keithley 6514) was connected between the power supply and emitter for floating potential measurement of the total current. The emitter is fixed onto a holder whereby temperature can be adjusted from 80 K to over 2,000 K using liquid nitrogen cooling and W filament joule heating.

Energy spread and brightness measurements. A hemispherical energy analyser (100 mm diameter, VG Scienta) was installed at a 90° angle to the micro-channel plate set with respect to the emitter. The probe current and energy spectrum were measured at sequential steps by rotating the emitter to target between the faraday cup and the energy analyser. The probe current was later converted into areal current density J after determining physical source size S_p by FIM. The energy analyser was operated at a constant pass energy of 18 eV and the energy scan was conducted by sweeping the retarding potential between the analyser and the entrance focusing optics. Transverse energy d is then extrapolated from energy spectrum taken at each probe current, which ranges from 200 pA to 21 nA. To obtain the exact work function value for the LaB_6 NW, a fitting of the spectrum like those shown in Fig. 2c was performed with[28]:

$$J(E - E_f) = N \cdot \frac{\exp((E - E_f)/d)}{1 + \exp((E - E_f)/kT)} \quad (3)$$

and

$$\phi = -1.64\frac{md}{U} \quad (4)$$

where N is a normalization constant, d is transverse energy, k_B is the Boltzmann constant and T is absolute temperature. A best fit of the spectrum was used to determine d and the I_t–U dependence was used to extrapolate the F–N slope m and y-intercept n.

The 'practical brightness' of the electron beam right after emitting from the emitter surface is defined as $B_r = I/\theta/S_v/U$, where I, θ, S_v and U are emission current, angular divergence, virtual source size that contains 50% of beam current, and beam potential, respectively. The practical brightness definition $B_r = 1.44J/(\pi d)$ (final form) was used to obtain the combined quantity B_r for each measurement. B_r and ΔE values for W(310), CNT and SAT were all taken from the literature where both values are available or could be deduced with provided data.

Two types of W needle were used for performance comparison measurements. A sharp W needle with a tip radius of around 30 nm was used for energy distribution measurements. The needle was not thermally annealed. Instead, ~6 kV field evaporation in vacuum was applied to remove surface contaminants to avoid thermal dulling of the emitter. In all other measurements, thermal annealing was applied to flash the W tip to ~2,000 °C till a clean FEM pattern of W appears. Tip radius expanded to about 100 nm after thermal annealing treatment. Electron emission from the (310) plane for all W needles were used in measurements.

An electron microscope using a LaB_6 nanowire emitter. A JSM-6700F field emission scanning electron microscope was used to carry out the comparison study with the original W(310) emitter and the LaB_6 NW emitter. To facilitate the low extraction voltage for the nanowire emitter, a customized high-stability power supply was specially made. LaB_6 NW emitter was mounted in the electron gun through an adaptor structure before chamber baking. Several mild flashings were then carried out and stable emission could be routinely obtained with LaB_6 NW emitter without any extractor degassing procedure. Prolonged extractor bombardment degassing was carried out after W(310) emitter installation to elongate its stable period. SEM images were recorded with a frame rate of 40 seconds per frame. For the chemical compositional mapping, an X-ray signal was acquired with count rate below 6 kps to ensure a detection dead time below 30% with the electron beam energy set at 15 kV and the working distance set at 15 mm.